

On the splitting of nucleon effective masses at high isospin density: reaction observables

M.Di Toro*, M.Colonna* and J.Rizzo*

**Laboratori Nazionali del Sud INFN, via S.Sofia 62, I-95123 Catania, Italy and Dipartimento di Fisica e Astronomia, Universita' di Catania*

Abstract. We review the present status of the nucleon effective mass splitting *puzzle* in asymmetric matter, with controversial predictions within both non-relativistic *and* relativistic approaches to the effective in medium interactions. Based on microscopic transport simulations we suggest some rather sensitive observables in collisions of asymmetric (unstable) ions at intermediate (*RIA*) energies: i) Energy systematics of Lane Potentials; ii) Isospin content of fast emitted nucleons; iii) Differential Collective Flows. Similar measurements for light isobars (like $^3H - ^3He$) could be also important.

ISOSPIN MOMENTUM DEPENDENCE IN SKYRME FORCES

We start from a discussion on the isospin dependence of these widely used non-relativistic effective interactions [1]. In a Skyrme-like parametrization the symmetry term has the form:

$$\varepsilon_{sym} \equiv \frac{E_{sym}}{A}(\rho) = \frac{\varepsilon_F(\rho)}{3} + \frac{C(\rho)}{2} \frac{\rho}{\rho_0} \quad (1)$$

with the function $C(\rho)$, in the potential part, given by:

$$\begin{aligned} \frac{C(\rho)}{\rho_0} = & -\frac{1}{4} \left[t_0(1+2x_0) + \frac{t_3}{6}(1+2x_3) \rho^\alpha \right] \\ & + \frac{1}{12} \left[t_2(4+5x_2) - 3t_1x_1 \right] \left(\frac{3\pi^2}{2} \right)^{2/3} \rho^{2/3} \equiv \frac{1}{\rho_0} \left[C_{Loc}(\rho) + C_{NLoc}(\rho) \right] \end{aligned} \quad (2)$$

with $\alpha > 0$ and the usual Skyrme parameters. We remark that the second term is related to isospin effects on the momentum dependence [2].

In the Fig. 1(left) we show the density dependence of the potential symmetry term of various Skyrme interactions, *SIII*, *SGII*, *SKM** (see [3] and refs. therein) and the more recent Skyrme-Lyon forms, *SLya* and *Slyb* (or *Sly4*), see [2, 4]. We also separately present the local and non-local contributions, first and second term of the Eq.(2). We clearly see a sharp change from the earlier Skyrme forces to the Lyon parametrizations, with almost an inversion of the signs of the two contributions, [5]. The important repulsive non-local part of the Lyon forces leads to a completely different behavior of the neutron matter , of great relevance for the neutron star properties. Actually this substantially modified parametrization was mainly motivated by a very unpleasant feature in the spin channel of the earlier Skyrme forces, the collapse of polarized neutron matter, see discussion in [8, 2, 4, 6]. In correspondence the predictions on the isospin effects on the momentum dependence of the symmetry term are quite different, see Fig.1 (left). A very important consequence for the reaction dynamics is the expected inversion of the sign of the n/p effective mass splitting.

Effective masses in neutron-rich matter

In asymmetric matter we consistently have a splitting of the neutron/proton effective masses given by:

$$m_q^{*-1} = m^{-1} + g_1\rho + g_2\rho_q, \quad (3)$$

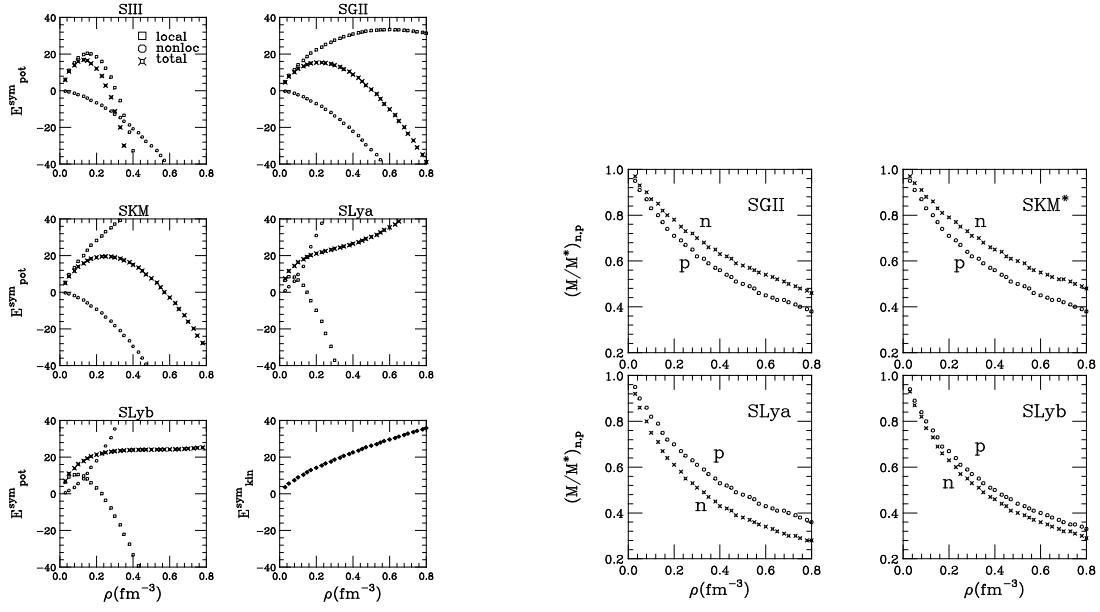


FIGURE 1. *Left:* Density dependence of the potential symmetry term for various Skyrme effective forces, see text. The bottom right panel shows the kinetic contribution. *Right:* Density dependence of the neutron/proton effective mass splitting for various Skyrme effective forces, see text. The asymmetry is fixed at $I = 0.2$, not very exotic.

with

$$\rho_{q=n,p} = \frac{1 \pm I}{2} \rho \quad (+, n).$$

The g_1 , g_2 coefficients are simply related to the momentum dependent part of the Skyrme forces:

$$\begin{aligned} g_1 &= \frac{1}{4\hbar^2} [t_1(2+x_1) + t_2(2+x_2)] \\ g_2 &= \frac{1}{4\hbar^2} [t_2(1+2x_2) - t_1(1+2x_1)] \end{aligned} \quad (4)$$

This result derives from a general q -structure of the momentum dependent part of the Skyrme mean field

$$U_{q,MD} = m(g_1\rho + g_2\rho_q)E \quad (5)$$

where E is the nucleon kinetic energy, while the total field seen by the q -nucleon has the form [7]

$$U_q(\rho, \rho_q, k) = U_{q,MD} + \frac{g_1\hbar^2\tau}{2} + \frac{g_2\hbar^2\tau_q}{2} + \frac{\partial \epsilon_{Loc}(Pot)}{\partial \rho_q} \quad (6)$$

where $\hbar^2\tau$ is the kinetic energy density and $\epsilon_{Loc}(Pot)$ the local part of the potential energy density.

In the Fig. 1(right) we show the density behavior of $m_{n,p}^*$ in neutron rich matter $I = 0.2$ for the same effective interactions. From the Eqs.(3, 4) we see that the sign of the g_2 univocally assigns the sign of the splitting, i.e. $g_2 < 0$ gives larger neutron masses $m_n^* > m_p^*$ while we have the opposite for $g_2 > 0$.

In the Table 1 we report some results obtained with various Skyrme forces for quantities of interest, around saturation, for the present discussion. We show also the E -slope of the corresponding Lane Potential, see later, simply related to the isospin dependent part of Eq.(5). For the effective mass parameters of Eq.(3) we observe that while the g_1 coefficients are always positive, corresponding to a decrease of the nucleon mass in the medium, the isospin dependent part shows different signs. In particular we see that in the Lyon forces the g_2 values are positive, with neutron effective masses below the proton ones for n-rich matter as shown in Fig. 1 (right).

TABLE 1. Properties at saturation

Force	<i>SIII</i>	<i>SGII</i>	<i>SkM*</i>	<i>SLya</i>	<i>SLy4</i>	<i>SLy7</i>
$g_1 (10^{-3}) (MeV^{-1} fm^3)$	+3.85	+3.31	+3.53	+10 ⁻⁵	+1.67	+1.70
$g_2 (10^{-3}) (MeV^{-1} fm^3)$	-3.14	-2.96	-3.50	+5.78	+2.53	+2.76
$\rho_0 (fm^{-3})$	0.150	0.1595	0.1603	0.160	0.1595	0.1581
$a_4 (MeV)$	28.16	26.83	30.03	31.97	32.01	32.01
$C(\rho_0) (MeV)$	31.72	29.06	35.46	39.40	39.42	39.42
$E - \text{slope} (\text{LanePot.})$	-0.22	-0.21	-0.26	+0.43	+0.19	+0.20

We note that the same is predicted from microscopic relativistic Dirac-Brueckner calculations [9, 10, 11] and in general from the introduction of scalar isovector virtual mesons in *RMF* approaches [12, 13]. At variance, non-relativistic Brueckner-Hartree-Fock calculations are leading to opposite conclusions [14, 16]. We remind that a comparison between relativistic effective (*Dirac*) masses and non-relativistic effective masses requires some attention. This point will be carefully discussed later.

Energy dependence of the Lane Potential

The sign of the splitting will directly affect the energy dependence of the Lane Potential, i.e. the difference between (n, p) optical potentials on charge asymmetric targets, normalized by the target asymmetry [17]. From the Eqs.(5,6) we obtain the explicit Skyrme form of the Lane Potential:

$$U_{Lane} \equiv \frac{U_n - U_p}{2I} = C(\rho_0) - \frac{2}{3}m\rho_0 \epsilon_F \left[g_1 + \frac{7}{12}g_2 \right] + \frac{m\rho_0}{2}g_2 E \quad (7)$$

where $C(\rho_0)$ gives the potential part of the a_4 parameter in the mass formula. We see that the $E - \text{slope}$ has just the sign of the g_2 parameter, and so we have opposite predictions from the various Skyrme forces analysed here. The change in the energy slope is reported in the last row of the Table 1. The difference in the energy dependence of the Lane Potential is quite dramatic.

The second term of the Eq.(7) is also interesting. In the case $g_2 > 0$ (positive slope) decreases the starting zero energy point, while in the case $g_2 < 0$ (negative slope) it represents a small correction to the symmetry energy $C(\rho_0)$. We then expect to see a *crossing* of the two prescriptions at very low energies, i.e. low momentum nucleons will see exactly the same Lane potentials.

An important physical consequence of the negative slopes is that the isospin effects on the optical potentials tend to disappear at energies just above 100 MeV (or even change the sign for “old” Skyrme-like forces). Unfortunately results derived from neutron/proton optical potentials at low energies are not conclusive, [17, 18, 19], since the effects appear of the same order of the uncertainty on the determination of the local contribution. Moreover at low energies we expect the crossing discussed before therefore for a wide energy range we cannot see differences. More neutron data are needed at higher energies, in particular a systematics of the energy dependence.

We can expect important effects on transport properties (fast particle emission, collective flows) of the dense and asymmetric *NM* that will be reached in Radioactive Beam collisions at intermediate energies, i.e. in the *RIA* energy range.

SYMMETRY ENERGY IN QUANTUM-HADRO-DYNAMICS

The *QHD* effective field model represents a very successful attempt to describe, in a fully relativistic picture, equilibrium and dynamical properties of nuclear systems at the hadronic level [20, 21, 22]. Here we focus on the dynamical response and static (equilibrium) properties of Asymmetric Nuclear Matter (*ANM*) in a “minimal” effective meson field model, with two meson (scalar and vector) contributions in each isospin channel, (σ, ω) for the isoscalar and (δ, ρ) for the isovector part, see details in [5] and refs. therein. In particular we will discuss the effects of the isovector/scalar δ meson, since this is directly related to the nucleon effective mass splitting of interest here.

The symmetry energy in ANM is defined from the expansion of the energy per nucleon $E(\rho_B, I)$ in terms of the asymmetry parameter $I \equiv -\frac{\rho_{B3}}{\rho_B} = \frac{\rho_{Bn} - \rho_{Bp}}{\rho_B} = \frac{N-Z}{A}$. We have

$$E(\rho_B, I) \equiv \frac{\varepsilon(\rho_B, I)}{\rho_B} = E(\rho_B) + E_{sym}(\rho_B)I^2 + O(I^4) + \dots \quad (8)$$

and so in general

$$E_{sym} \equiv \frac{1}{2} \frac{\partial^2 E(\rho_B, I)}{\partial I^2} \Big|_{I=0} = \frac{1}{2} \rho_B \frac{\partial^2 \varepsilon}{\partial \rho_B^2} \Big|_{\rho_B=0} \quad (9)$$

In the Hartree case an explicit expression for the symmetry energy is easily derived that can be reduced to a very simple form, with transparent δ -meson effects [12, 13]:

$$E_{sym}(\rho_B) = \frac{1}{6} \frac{k_F^2}{E_F^*} + \frac{1}{2} \left[f_\rho - f_\delta \left(\frac{m^*}{E_F^*} \right)^2 \right] \rho_B \quad (10)$$

where k_F is the nucleon Fermi momentum corresponding to ρ_B , $E_F^* \equiv \sqrt{(k_F^2 + m^*^2)}$ and m^* is the effective nucleon mass in symmetric NM , $m^* = m + \Sigma_s(\sigma)$, with the isoscalar, scalar self-energy $\Sigma_s(\sigma) \equiv -f_\rho \rho_s$ (ρ_s scalar density). $f_i \equiv (\frac{s_i}{m_i})^2$, $i = \sigma, \omega, \delta, \rho$, are the effective meson coupling constants [24].

We see that, when the δ is included, the empirical a_4 value actually corresponds to the combination $[f_\rho - f_\delta(\frac{M}{E_F})^2]$ of the (ρ, δ) coupling constants. Therefore if $f_\delta \neq 0$ we have to increase correspondingly the ρ -coupling.

Now the symmetry energy at saturation density is actually built from the balance of scalar (attractive) and vector (repulsive) contributions, with the scalar channel becoming weaker with increasing baryon density. This is clearly shown in Fig.2(left). This is indeed the isovector counterpart of the saturation mechanism occurring in the isoscalar channel for symmetric nuclear matter.

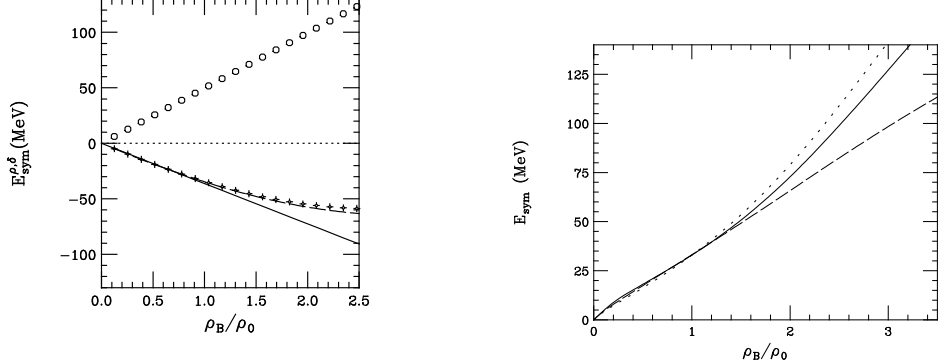


FIGURE 2. Left: ρ - (open circles) and δ - (crosses) contributions to the potential symmetry energy. The solid line is a linear extrapolation of the low density δ contribution. Right: Total (kinetic + potential) symmetry energy as a function of the baryon density. Dashed line ($NL\rho$). Dotted line ($NL\rho\delta$). Solid line $NLHF$, only Fock correlations [13].

In Fig.2(right) we show the total symmetry energy for the different models. At subnuclear densities, $\rho_B < \rho_0$, in both cases, $NL\rho$ and $NL\rho\delta$, from Eq.(10) we have an almost linear dependence of E_{sym} on the baryon density, since $m^* \simeq E_F$ as a good approximation. Around and above ρ_0 we see a steeper increase in the $(\rho + \delta)$ case since m^*/E_F is decreasing.

In conclusion when the δ -channel is included the behaviour of the symmetry energy is stiffer at high baryon density from the relativistic mechanism discussed before. This is in fact due to a larger contribution from the ρ relative to the δ meson. We expect to see these effects more clearly in the relativistic reaction dynamics at intermediate energies, where higher densities are reached.

Nucleon Effective Mass Splitting

An important qualitatively new result of the δ -meson coupling is the n/p -effective mass splitting in asymmetric matter, [5] and refs. therein, *Dirac* mass, see later:

$$m_D^*(q) = m + \Sigma_s(\sigma) \pm f_\delta \rho_{S3} , \quad (11)$$

where $+$ is for neutrons. Since $\rho_{S3} \equiv \rho_{Sp} - \rho_{Sn}$, in n -rich systems we have a neutron *Dirac* effective mass always smaller than the proton one. We note again that a decreasing neutron effective mass in n -rich matter is a direct consequence of the relativistic mechanism for the symmetry energy, i.e. the balance of scalar (attractive) and vector (repulsive) contributions in the isovector channel.

Dirac and Schrödinger Nucleon Effective Masses in Asymmetric Matter

The prediction of a definite $m_D^*(n) < m_D^*(p)$ effective mass splitting in *RMF* approaches, when a scalar δ -*like* meson is included, is an important result that requires some further analysis, in particular relative to the controversial predictions of non-relativistic approaches.

Here we are actually discussing the *Dirac* effective masses $m_D^*(n, p)$, i.e. the effective mass of a nucleon in the in-medium *Dirac* equation with all the meson couplings. The relation to the *Schrödinger* effective masses $m_S^*(n, p)$, i.e. the “ k -mass” due to the momentum dependence of the mean field in the non-relativistic in-medium *Schrödinger* equation is not trivial, see [25, 21, 26, 27]. We will extend the argument of the refs. [26, 27] to the case of asymmetric matter.

We start from the simpler symmetric case without self-interacting terms. The nucleon *Dirac* equation in the medium contains the scalar self-energy $\Sigma_s = -f_\sigma \rho_S$ and the vector self-energy (fourth component) $\Sigma_0 = f_\omega \rho_B$ and thus the corresponding energy-momentum relation reads:

$$(\varepsilon + m - \Sigma_0)^2 = p^2 + (m + \Sigma_s)^2 = p^2 + m_D^{*2} \quad (12)$$

i.e. a dispersion relation

$$\varepsilon = -m + \Sigma_0 + \sqrt{p^2 + m_D^{*2}} \quad (13)$$

From the total single particle energy $E = \varepsilon + m$ expressed in the form $E = \sqrt{k_\infty^2 + m^2}$, where k_∞ is the relativistic asymptotic momentum, using Eq.(12) we can get the relation

$$\begin{aligned} \frac{k_\infty^2}{2m} &= \varepsilon + \frac{\varepsilon^2}{2m} = \\ \frac{p^2}{2m} + \Sigma_s + \Sigma_0 + \frac{1}{2m}(\Sigma_s^2 - \Sigma_0^2) + \frac{\Sigma_0}{m}\varepsilon &\equiv \frac{p^2}{2m} + U_{eff}(\rho_B, \rho_s, \varepsilon) \end{aligned} \quad (14)$$

i.e. a *Schrödinger*-type equation with a momentum dependent mean field that with the dispersion relation Eq.(13) is written as

$$\begin{aligned} U_{eff} &= \Sigma_s + \frac{1}{2m}(\Sigma_s^2 + \Sigma_0^2) + \frac{\Sigma_0}{m}\sqrt{(p^2 + m_D^{*2})} \\ &\simeq \Sigma_s + \frac{\Sigma_0 m_D^*}{m} + \frac{1}{2m}(\Sigma_s^2 + \Sigma_0^2) + \frac{p^2}{2m} \frac{\Sigma_0}{m_D^*} \end{aligned} \quad (15)$$

The relation between *Schrödinger* and *Dirac* nucleon effective masses is then

$$m_S^* = \frac{m}{1 + \frac{\Sigma_0}{m_D^*}} = m_D^* \frac{m}{m + \Sigma_s + \Sigma_0} \quad (16)$$

Since at saturation the two self-energies are roughly compensating each other, $\Sigma_s + \Sigma_0 \simeq -50 MeV$ the two effective masses are not much different, with the S -*mass* slightly larger than the D -*mass*.

In the case of asymmetric matter, neutron-rich as always considered here, we can have two cases:

- *Only ρ meson coupling*

Now the scalar part is not modified, we have the same scalar self energies Σ_s for neutrons and protons and so the same Dirac masses. The vector self energies will show an isospin dependence with a new term $\mp f_\rho \rho_{B3}$, repulsive for neutrons (– sign, since we use the definition $\rho_{(B,S)3} \equiv \rho_{(B,S)p} - \rho_{(B,S)n}$). As a consequence we see a splitting at the level of the Schrödinger masses since Eq.(16) becomes

$$m_S^*(n, p) = m_D^* \frac{m}{m + (\Sigma_s + \Sigma_0)_{sym} \mp f_\rho \rho_{B3}} \quad (17)$$

in the direction of $m_S(n)^* < m_S(p)^*$ (here and in the following upper signs are for neutrons).

- *$\rho + \delta$ coupling*

The above splitting is further enhanced by the direct effect of the scalar isovector coupling, see Eq.(11). Then the Schrödinger masses are

$$m_S^*(n, p) = (m_{D_{sym}}^* \pm f_\delta \rho_{S3}) \frac{m}{m + (\Sigma_s + \Sigma_0)_{sym} \mp (f_\rho \rho_{B3} - f_\delta \rho_{S3})} \quad (18)$$

The new term in the denominator will further contribute to the $m_S^*(n) < m_S^*(p)$ splitting since we must have $f_\rho > f_\delta$ in order to get a correct symmetry parameter a_4 . The effect is larger at higher baryon densities because of the decrease of the scalar ρ_{S3} , due to the faster $\frac{m_{Dn}^*}{E_{Fn}^*}$ reduction of ρ_{Sn} .

Actually in a non-relativistic limit we can approximate in Eq.(14) directly the energy ε with the asymptotic kinetic energy leading to the much simpler relation:

$$m_S^* = \frac{m}{1 + \frac{\Sigma_0}{m}} \simeq m - \Sigma_0 = m_D^* - (\Sigma_s + \Sigma_0). \quad (19)$$

In the case of asymmetric matter this leads to the more transparent relations

- *Only ρ meson coupling*

$$m_S^*(n, p) = m_D^* - (\Sigma_s + \Sigma_0)_{sym} \pm f_\rho \rho_{B3} \quad (20)$$

- *$\rho + \delta$ coupling*

$$m_S^*(n, p) = m_{D_{sym}}^* - (\Sigma_s + \Sigma_0)_{sym} \pm (f_\rho \rho_{B3} - f_\delta \rho_{S3}) \quad (21)$$

In conclusion any *RMF* model will predict the definite isospin splitting of the nucleon effective masses $m_S(n)^* < m_S(p)^*$ in the non-relativistic limit. We expect an increase of the difference of the neutron/proton mean field at high momenta, with important dynamical contributions that will enhance the transport effects of the symmetry energy.

Beyond RMF: k -dependence of the Self-Energies

Correlations beyond the Mean Field picture will lead to a further density and, most important, momentum dependence of the effective couplings and consequently of the Self-Energies. This can be clearly seen from microscopic Dirac-Brueckner (*DBHF*) calculations, see [9, 10, 11] and refs. therein. Even the basic Fock correlations are implying a density dependence of the couplings, see [13]. In fact from the very first relativistic transport calculations a momentum dependence of the vector fields was required in order to reduce the too large repulsion of the optical potential at high momenta, see [28]. From the above discussion we can expect that, when the δ -meson is included [29], the sign of the *Dirac*-mass splitting will not be modified, i.e. $m_{Dn}^* < m_{Dp}^*$. In fact this is the result of the microscopic *DBHF* calculations in asymmetric matter of refs.[9, 10, 11]. The problem is however that in correspondence the Schrödinger mass splitting can have any sign. Indeed this is the case of the very recent *DBHF* analysis of the Tübingen group [11, 30]. For the *S*-masses they get an opposite behavior $m_{Sn}^* > m_{Sp}^*$, with large fluctuations around the Fermi momenta, due to the opening of the phase space for intermediate inelastic channels. These results are actually dependent on the way the self-energies (mean fields) are derived from the full correlated theory and different predictions can be obtained, see the recent refs.[31, 32, 33].

All that clearly shows that experimental observables are in any case strongly needed.

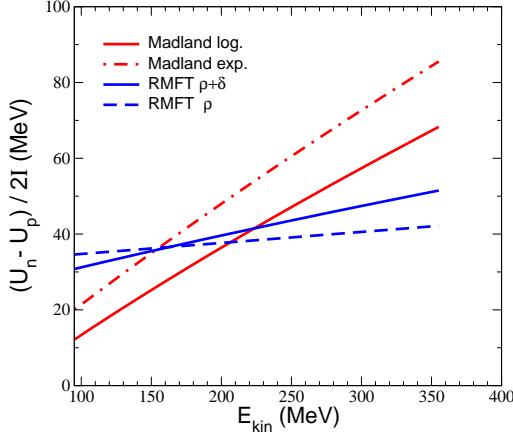


FIGURE 3. Energy dependence of the Dirac-Lane potential in the RMF picture (solid: $NL\rho$; dashed: $NL\rho\delta$) and in the phenomenologic Dirac Optical Model of Madland et al. [37, 38], see text.

The Dirac-Lane Potential

In the non-relativistic limit of the Eq.(14) we can easily extract the neutron-proton mean optical potential using the isospin dependence of the self-energies

$$\begin{aligned}\Sigma_{0,q} &= \Sigma_{0,sym} \mp f_\rho \rho_{B3} , \\ \Sigma_{s,q} &= \Sigma_{s,sym} \pm f_\delta \rho_{S3} ,\end{aligned}\quad (22)$$

With some algebra we get a compact form of the *Dirac – Lane Potential*

$$\begin{aligned}U_{Dirac-Lane} &\equiv \frac{U_n - U_p}{2I} = \\ \rho_0 \left[f_\rho \left(1 - \frac{\Sigma_{0,sym}}{m} \right) - f_\delta \frac{\rho_{S3}}{\rho_{B3}} \left(1 + \frac{\Sigma_{s,sym}}{m} \right) \right] + f_\rho \frac{\rho_0}{m} \varepsilon\end{aligned}\quad (23)$$

It is interesting to compare with the related discussion presented for the non-relativistic effective forces, mainly of Skyrme-like form. First of all we predict a definite positive $E - slope$ given by the quantity $f_\rho \frac{\rho_0}{m}$, which is actually not large within the simple *RMF* picture described here. This is a obvious consequence of the fact that the “relativistic” mass splitting is always in the direction $m_S(n)^* < m_S(p)^*$. The realistic magnitude of the effect could be different if we take into account that some explicit momentum dependence should be included in the scalar and vector self energies, [28], as also discussed before. An interesting point in this direction comes from the phenomenological Dirac Optical Potential (*Madland – potential*) constructed in the refs. [37, 38], fitting simultaneously proton and neutron (mostly total cross sections) data for collisions with a wide range of nuclei at energies up to 100 MeV. Recently this Dirac optical potential has been proven to reproduce very well the new neutron scattering data on ^{208}Pb at 96 MeV [39] measured at the Svendborg Laboratory in Uppsala.

The phenomenological *Madland – potential* has different implicit momentum dependences (*exp/log*) in the self-energies, [37, 38]. In Fig.3 we show the corresponding energy dependences for the *Dirac – Lane* potentials, compared to our $NL\rho$ and $NL\rho\delta$ estimations. When we add the δ -field we have a larger slope since the ρ – coupling should be increased. The slopes of the phenomenological potentials are systematically larger, interestingly similar to the ones of the *Skyrme – Lyon* forces. We note that in the *Madland – potential* the Coulomb interaction is included, i.e. an extra repulsive vector contribution for the protons. The first, not energy dependent, term of Eq.(23) is directly related to the symmetry energy at saturation, exactly like in the non-relativistic case, see Eq.(7).

The conclusion is that a good *systematic* measurement of the Lane potential in a wide range of energies, and particularly around/above 100 MeV, would answer many fundamental questions in isospin physics.

REACTION OBSERVABLES

In order to directly test the influence of the S -effective mass splitting we will present results from reaction dynamics at intermediate energies analysed in a non-relativistic transport approach, of *BNV* type, see [5]. The *Iso*–*MD* effective interaction is derived via an asymmetric extension of the *GBD* force, [34, 35], constructed in order to have a strict correspondence to the Skyrme forces, see also [36].

The energy density can be parametrized as follows:

$$\varepsilon = \varepsilon + \varepsilon_{kin} + \varepsilon(A', A'') + \varepsilon(B', B'') + \varepsilon(C', C'') \quad (24)$$

where ε_{kin} is the usual kinetic energy density and

$$\begin{aligned} \varepsilon(A', A'') &= (A' + A''\beta^2) \frac{\rho^2}{\rho_0} \\ \varepsilon(B', B'') &= (B' + B''\beta^2) \left(\frac{\rho}{\rho_0} \right)^\sigma \rho \\ \varepsilon(C', C'') &= C'(\mathcal{I}_{NN} + \mathcal{I}_{PP}) + C''\mathcal{I}_{NP} \end{aligned} \quad (25)$$

Here $\mathcal{I}_{\tau\tau'}$ are integrals of the form:

$$\mathcal{I}_{\tau\tau'} = \int d\vec{p} d\vec{p}' f_\tau(\vec{r}, \vec{p}) f_{\tau'}(\vec{r}, \vec{p}') g(\vec{p}, \vec{p}')$$

with $g(\vec{p}, \vec{p}') = g(\vec{p} - \vec{p}')^2$. This choice of the function $g(\vec{p}, \vec{p}')$ corresponds to a Skyrme-like behaviour and it is suitable for *BNV* simulations. In this frame we can easily adjust the parameters in order to have the same density dependence of the symmetry energy *but with two opposite n/p effective mass splittings*. So we can separately study the correspondent dynamical effects, [36]. In Fig. 4 we show the E -dependence of the Lane potentials with the parametrizations corresponding to the two choices of the sign of the n/p mass splitting (shown in the insert for the $I = 0.2$ asymmetry). The value of the splitting is exactly the same, only the sign is opposite.

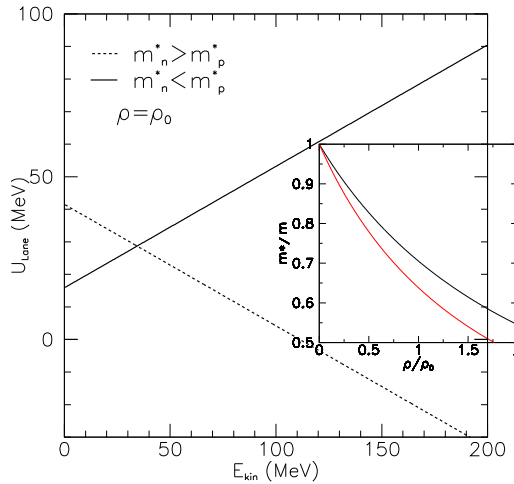


FIGURE 4. Lane potential for the used parametrizations; small panel: the effective mass splitting, related to the slope of the Lane potential.

The upper curve well reproduces the Skyrme-Lyon (in particular *SLy4*, *Sly7*) results. The lower (dashed) the *SIII*, *SKM** ones. We clearly see the crossing at low energy, as expected from the previous discussion.

From the figure we can immediately derive the expectation of very different symmetry effects for nucleons around 100 MeV kinetic energy, enhancement (with larger neutron repulsion) in the $m_n^* < m_p^*$ case vs. a disappearing (and even larger proton repulsion) in the $m_n^* > m_p^*$ choice. So it seems natural to look at observables where neutron/proton mean fields at high momentum are playing an important role. We will show results for fast nucleon emissions and collective flows at intermediate energies, in particular for high transverse momentum selections.

Isotopic content of the fast nucleon emission

We have performed realistic “ab initio” simulations of collisions at intermediate energies of n-rich systems, in particular $^{132}\text{Sn} + ^{124}\text{Sn}$ at 50 and 100,AMeV, central selection. Performing a local low density selection of the test particles ($\rho < \rho_0/8$) we can follow the time evolution of nucleon emissions (gas phase) and the corresponding asymmetry. In Fig. 5 we show the evolution of the gas asymmetry ($I(t) \equiv (N - Z)/A$) for the 50AMeV reaction (the solid line gives the initial asymmetry). For both choices of the density stiffness of the symmetry term we clearly see the effects of the mass splitting, resulting in a reduced fast neutron emission when $m_n^* > m_p^*$.

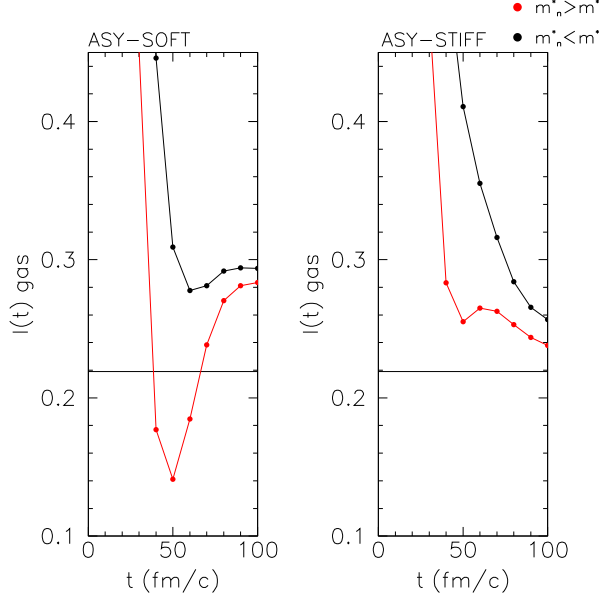


FIGURE 5. Isospin gas content as a function of time in a central collision $^{132}\text{Sn} + ^{124}\text{Sn}$ at 50AMeV for two opposite choices of mass splitting. Left: asy-soft EOS; right: asy-stiff EOS.

In order to better disentangle the mass splitting effect and to select the corresponding observables, in Figs. 6, 7 we report the N/Z of the “gas” at two different times, $t = 60\text{ fm}/c$, end of the pre-equilibrium emission, and $t = 100\text{ fm}/c$ roughly freeze out time. We have followed the transverse momentum dependence, for a fixed central rapidity $y(0)$ (normalized to projectile rapidity). In Fig. 6 we show the results *without the mass splitting effect*, i.e. only taking into account the different repulsion of the symmetry term (the intial average asymmetry is $N/Z = 1.56$).

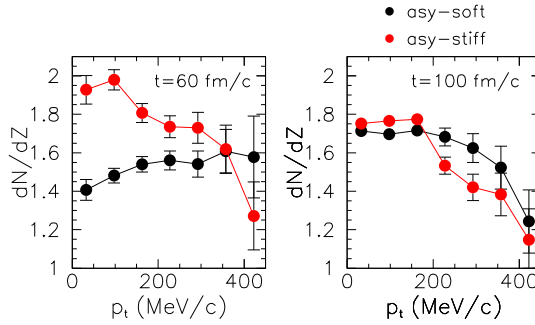


FIGURE 6. Transverse momentum dependence of the neutron/proton ratio in the rapidity range $|y(0)| \leq 0.3$ for a central reaction $^{132}\text{Sn} + ^{124}\text{Sn}$ at 50AMeV. Comparison between two choices of symmetry energy stiffness at different times.

At early times (left panel of Fig. 6), when the emission from high density regions is dominant, we see a difference due to the larger neutron repulsion of the the asy-stiff choice. The effect is reduced at higher p_t s due to the overall repulsion of the isoscalar momentum dependence. Finally at freeze out (right panel) the difference is almost dis-

pearing even for the more efficient *Isospin Distillation* of the asy-soft choice during the expansion phase, [5] and refs. therein.

When we introduce the mass splitting the difference in the isotopic content of the gas, for the larger transverse momenta, is very evident at all times, in particular at the freeze-out of experimental interest, see Fig. 7. As expected the $m_n^* > m_p^*$ sharply reduces the neutron emission at high p_t s.

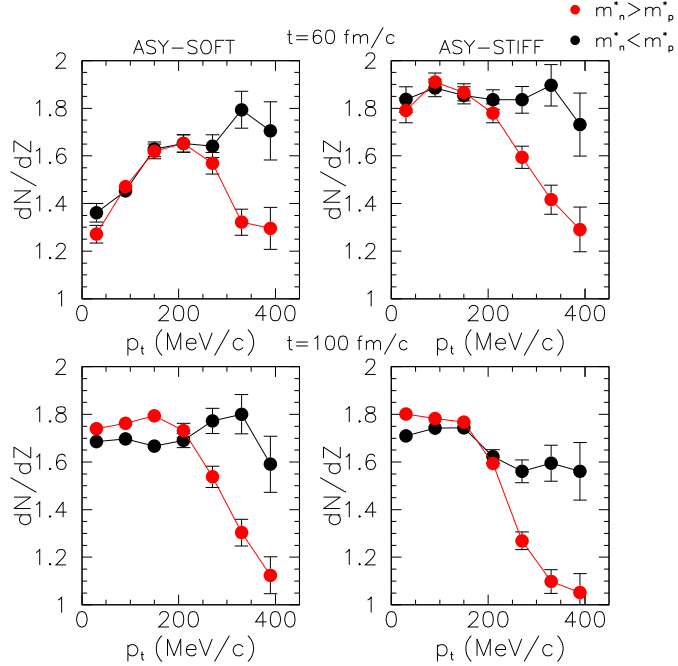


FIGURE 7. Same as Fig. 6, for two opposite choices of mass splitting.

We have repeated the analysis at higher energy, 100AMeV, and the effect appears nicely enhanced, see Fig. 8.

Similar results have been obtained in ref. [40] at 400AMeV in a different *Iso – MD* model, restricted to the $m_n^* > m_p^*$ choice. In conclusion it appears that the isospin content of pre-equilibrium emitted nucleons at high transverse momentum can solve the mass-splitting puzzle.

Differential collective flows and mass splittings

Collective flows are expected to be very sensitive to the momentum dependence of the mean field, see [5] and refs.therein. We have then tested the isovector part of the momentum dependence just evaluating the *Differential* transverse and elliptic flows

$$V_{1,2}^{(n-p)}(y, p_t) \equiv V_{1,2}^n(y, p_t) - V_{1,2}^p(y, p_t)$$

at various rapidities and transverse momenta in semicentral ($b/b_{max} = 0.5$) $^{197}Au + ^{197}Au$ collisions at 250AMeV, where some proton data are existing from the *FOPI* collaboration at *GSI* [41, 42].

Transverse flows

For the differential transverse flows, see Fig. 9 the mass splitting effect is evident at all rapidities, and nicely increasing at larger rapidities and transverse momenta, with more neutron flow when $m_n^* < m_p^*$.

Just to show that our simulations give realistic results we compare in lower right panel of Fig. 9 with the proton data of the *FOPI* collaboration for similar selections of impact parameters rapidities and transverse momenta.

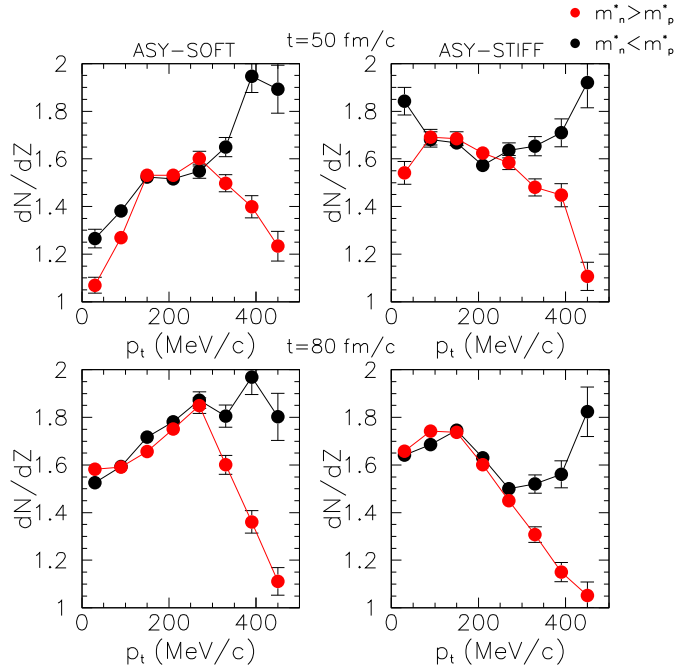


FIGURE 8. Same as Fig. 7, but for an incident energy of 100 AMeV.

The agreement is quite satisfactory. We see a slightly reduced proton flow at high transverse momenta in the $m_n^* < m_p^*$ choice, but the effect is too small to be seen from the data. Our suggestion of the differential flows looks much more promising.

Elliptic flows

The same analysis has been performed for the differential elliptic flows, see Fig. 10. Again the mass splitting effects are more evident for higher rapidity and transverse momentum selections. In particular the differential elliptic flow becomes systematically negative when $m_n^* < m_p^*$, revealing a faster neutron emission and so more neutron squeeze out (more spectator shadowing).

In the lower right panel we also show a comparison with recent proton data from the *FOPI* collaboration. The agreement is still satisfactory. As expected the proton flow is more negative (more proton squeeze out) when $m_n^* > m_p^*$. It is however difficult to draw definite conclusions only from proton data.

Again the measurement of differential flows appears essential. This could be in fact an experimental problem due to the difficulties in measuring neutrons. Our suggestion is to measure the difference between light isobar flows, like triton vs. 3He and so on. We expect to clearly see the effective mass splitting effects, maybe even enhanced due to larger overall flows, see [5, 43].

REFERENCES

1. D.Vautherin and D.M.Brink, Phys.Rev. C3 (1972) 676.
2. E.Chabanat, P.Bonche, P.Haensel, J.Meyer, R.Schaeffer, Nucl.Phys. A627 (1997) 710.
3. H.Krivine, J.Treiner and O.Bohigas, Nucl.Phys. A336 (1980) 155.
4. E.Chabanat, P.Bonche, P.Haensel, J.Meyer, R.Schaeffer, Nucl.Phys. A635 (1998) 231.
5. V.Baran, M.Colonna, V.Greco, M.Di Toro, Physics Reports 410 (2005) 335-466.
6. F.Douchin, P.Haensel and J.Meyer, Nucl.Phys. A665 (2000) 419.
7. M.Colonna, M.Di Toro, A.Larionov, Phys.Lett. B428 (1998) 1.
8. M.Kutschera, W.Wojcik, Phys.Lett. B325 (1994) 217.

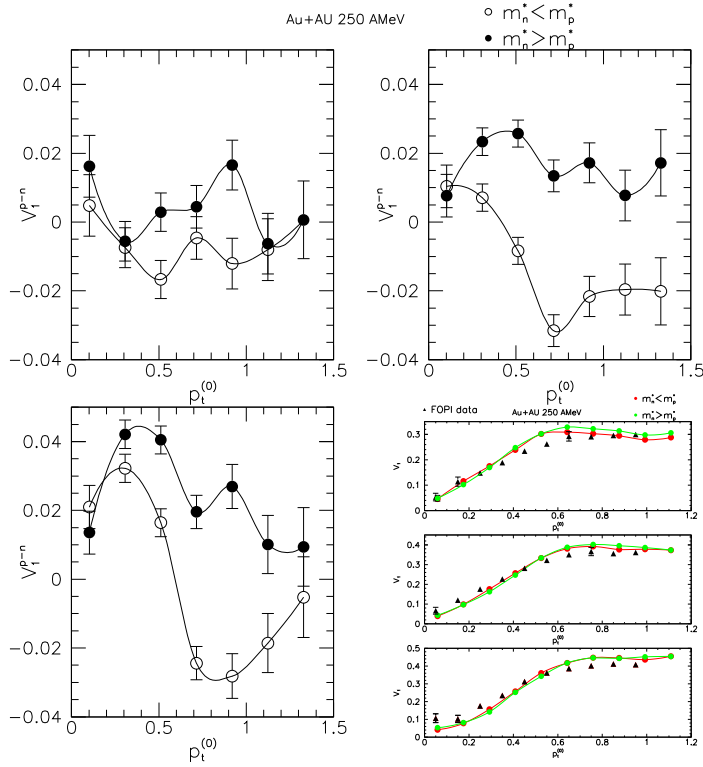


FIGURE 9. Difference between proton and neutron V_1 flows in a semi-central reaction $Au+Au$ at 250 AMeV for three rapidity ranges. Upper Left Panel: $|y^{(0)}| \leq 0.3$; Upper Right: $0.3 \leq |y^{(0)}| \leq 0.7$; Lower Left: $0.6 \leq |y^{(0)}| \leq 0.9$. Lower Right Panel: Comparison of the V_1 proton flow with FOPI data [41] for three rapidity ranges. Top: $0.5 \leq |y^{(0)}| \leq 0.7$; center: $0.7 \leq |y^{(0)}| \leq 0.9$; bottom: $0.9 \leq |y^{(0)}| \leq 1.1$.

9. F.Hofmann, C.M.Keil, H.Lenske, Phys.Rev. C64 (2001) 034314 .
10. E.Schiller, H.Müther, Eur.Phys.J. A11 (2001) 15.
11. E.N.E.van Dalen, C.Fuchs, A.Faessler, Nucl.Phys. A744 (2004) 227.
12. B.Liu, V.Greco, V.Baran, M.Colonna, M.Di Toro, Phys.Rev. C65 (2002) 045201.
13. V.Greco, M.Colonna, M.Di Toro, F.Matera, Phys.Rev. C67 (2003) 015203.
14. I.Bombaci, "EOS for isospin-asymmetric nuclear matter for astrophysical applications", in [15] pp. 35-81 and refs. therein.
15. *Isospin Physics in Heavy-ion Collisions at Intermediate Energies*, Eds. Bao-An Li and W. Udo Schröder, Nova Science Publishers (2001, New York).
16. W.Zuo, I.Bombaci, U.Lombardo, Phys.Rev. C60 (1999) 24605.
17. A.M.Lane, Nucl.Phys. 35 (1962) 676.
18. F.D.Becchetti, G.W.Greenless, Phys.Rev. 182 (1969) 1190.
19. P.E.Hodgson, *The Nucleon Optical Model*, World Scientific, 1994
20. J.D.Walecka, Ann.Phys.(N.Y.) 83 (1974) 491.
21. B.D.Serot, J.D.Walecka in *Advances in Nuclear Physics* Vol. 16, Eds. J.M.Negele and E.Vogt, Plenum, New York, 1986.
22. B.D.Serot, J.D.Walecka, Int.J.Mod.Phys. E6 (1997) 515.
23. S.Kubis, M.Kutschera, Phys.Lett. B399 (1997) 191.
24. The $NL\rho$, $NL\rho\delta$ parametrizations used here have been derived from transport studies of relativistic heavy ion collisions, see Ch.8 of ref. [5].
25. A.Bouyssy, J.F.Mathiot, N.Van Giai and S.Marcos, Phys.Rev. C36 (1987) 380.
26. M.Jaminon, C.Mahaux, P.Rochus, Phys.Rev. C22 (1980) 2027.
27. M.Jaminon, C.Mahaux, Phys.Rev. C40 (1989) 354.
28. B.Blättel, V.Koch and U.Mosel, Rep.Prog.Phys. 56 (1993) 1.
29. We like to remind that an isovector scalar channel in the effective interaction "automatically" appear when correlations are accounted for, see discussion in [5].
30. E. van Dalen, C.Fuchs, A.Fässler, *Effective Nucleon Masses in Symmetric and Asymmetric Nuclear Matter*, arXiv:nucl-th/0502064.
31. Z-Y.Ma et al., Phys.Lett. B606 (2004) 170.
32. D.Alonso and F.Sammarruca, arXiv:nucl-th/0301032

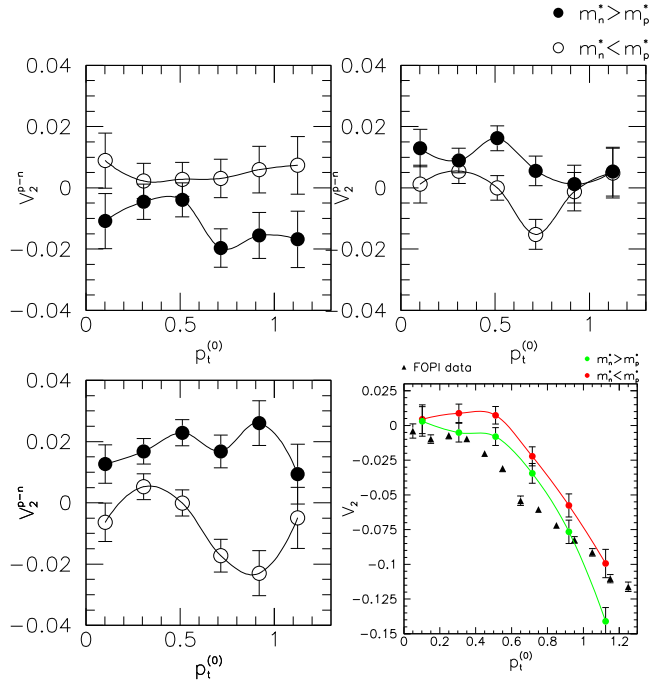


FIGURE 10. *Upper (left and right) and lower left panels: Difference between proton and neutron elliptic flows for the same reaction and rapidity ranges as in Fig. 9. Lower right panel: Comparison of the elliptic proton flow with FOPI data [42] (M3 centrality bin, $|y^{(0)}| \leq 0.1$).*

33. F.Sammarruca, W.Barredo, P.Krastev, arXiv:nucl-th/0411053v2.
34. C.Gale, G.F.Bertsch, S.Das Gupta, Phys.Rev. C41 (1990) 1545.
35. V.Greco, Diploma Thesis (1997);
V.Greco, A.Guarnera, M.Colonna, M.Di Toro, Phys.Rev. C59 (1999) 810.
Nuovo Cimento A111 (1998) 865.
36. J.Rizzo, M.Colonna, M.Di Toro, V.Greco, Nucl.Phys. A732 (2004) 202.
37. R.Kozack, D.G.Madland, Phys.Rev. C39 (1989) 1461.
38. R.Kozack, D.G.Madland, Nucl.Phys. A509 (1990) 664.
39. J.Klug et al., Phys.Rev. C67 (2003) 0316001R
ibidem Phys.Rev. C68 (2003) 064605.
40. B.-A.Li, C.B.Das, S.Das Gupta, C.Gale, Nucl.Phys. A735 (2004) 563.
41. A.Andronic et al., FOPI Collab., Phys.Rev. C67 (2003) 034907.
42. A.Andronic et al., FOPI Collab., Phys.Lett. B612 (2005) 173.
43. L.Scalone, M.Colonna, M.Di Toro, Phys.Lett. B461 (1999) 9.